Progress towards implementing superdense teleportation in Space

Chapman, Joseph, Bernstein, Herbert, Meier, Kristina, Zeitler, Chris, Kwiat, Paul

Joseph C. Chapman, Herbert Bernstein, Kristina Meier, Chris Zeitler, Paul G. Kwiat, "Progress towards implementing superdense teleportation in Space," Proc. SPIE 10547, Advances in Photonics of Quantum Computing, Memory, and Communication XI, 105470E (22 February 2018); doi: 10.1117/12.2295042

SPIE.

Event: SPIE OPTO, 2018, San Francisco, California, United States

Progress Towards Implementing Superdense Teleportation in Space

Joseph C. Chapman*[a], Herbert Bernstein[b], Kristina Meier[a], Chris Zeitler[a], and Paul G. Kwiat[a]
[a]University of Illinois, Dept. of Physics, Urbana, IL,USA,
[b] Hampshire College, School of Natural Science & ISIS Institute, Amherst, MA, USA

ABSTRACT

Superdense Teleportation (SDT) is a suitable protocol to choose for an advanced demonstration of quantum communication in space. We have taken further steps towards the realization of SDT in such an endeavor. Our system uses polarization and time-bin hyperentanglement via non-degenerate spontaneous parametric downconversion to implement SDT of 4-dimensional equimodular states. Previously, we have shown high fidelity (>90%) SDT implementation and the feasibility to perform SDT on an orbiting platform by correcting the Doppler shift. Here we discuss new analysis of the received state reconstruction performance in the presence of high channel loss and multiple pair events. Additionally, initial characterization of a waveguide-based entanglement source intended for space will be presented.

Keywords: hyperentanglement, quantum communication, superdense teleportation, multiple photon pairs, waveguide

1. INTRODUCTION

It has become apparent that fiber or terrestrial free-space optical links are unsuitable for quantum communication over large terrestrial distances without requiring many high-efficiency quantum repeaters. However, a link between a party in orbit, e.g., the International Space Station (ISS), and one on Earth is favorable due to decreased channel loss and turbulence compared to other links over similar distances[1,2]. We have therefore developed a system to execute superdense teleportation (SDT), a protocol we believe is a prime candidate for such a space-to-earth link.

2. SUPERDENSE TELEPORTATION

2.1 Protocol Description

SDT is a protocol[3] involving three parties, Alice, Bob, and Charles, in which Charles wishes to send Bob a particular d-dimensional equimodular state, characterized by d-1 arbitrary phases:

$$|\psi_C\rangle = \frac{1}{\sqrt{d}}(|0\rangle + |1\rangle e^{i\varphi_1} + |2\rangle e^{i\varphi_2} + \ldots + |d-1\rangle e^{i\varphi_{d-1}}). \quad (1)$$

Charles and Bob initially share a d-dimensional entangled state

$$|\psi_{BC}\rangle = \frac{1}{\sqrt{d}}(|00\rangle + |11\rangle + |22\rangle + \ldots + |(d-1)(d-1)\rangle); \quad (2)$$

Charles locally changes the phases between the terms of the nonlocal state to match those he wishes to teleport to Bob. Alice then measures Charles' half of the state in a basis which is mutually unbiased to the basis in which Charles applied the phases. Finally, she transmits the result of the projection measurement to Bob, who can deterministically apply the correct unitary transformation to finish preparing the state Charles desired to send.

2.2 Protocol Implementation

SDT has previously been implemented with photons hyperentangled in their polarization and orbital angular momentum degrees of freedom[4]. In our experiment, the logical states ($|0\rangle$, $|1\rangle$, $|2\rangle$, and $|3\rangle$) are encoded using photon polarization ($|H\rangle$ or $|V\rangle$) and time bins ($|t_1\rangle$ or $|t_2\rangle$): $|0\rangle \equiv |\mathrm{H}\rangle|\mathrm{t}_1\rangle$, $|1\rangle \equiv |\mathrm{V}\rangle|\mathrm{t}_1\rangle$, $|2\rangle \equiv |\mathrm{H}\rangle|\mathrm{t}_2\rangle$, and $|3\rangle \equiv |\mathrm{V}\rangle|\mathrm{t}_2\rangle$. The setup used to

* jchapmn2@illinois.edu; phone: 1-217-244-1608

Advances in Photonics of Quantum Computing, Memory, and Communication XI, edited by Zameer Ul Hasan, Philip R. Hemmer, Alan E. Craig, Alan L. Migdall, Proc. of SPIE Vol. 10547
105470E · © 2018 SPIE · CCC code: 0277-786X/18/$18 · doi: 10.1117/12.2295042

execute SDT is shown in Figure 1. A periodically-poled lithium niobate crystal (PPLN) is pumped by a 532-nm, 80-MHz mode-locked laser producing ~ 5-ps FWHM pulses. The PPLN can spontaneously produce pairs of polarization-entangled photons at 810 nm and 1550 nm via type-0 spontaneous parametric downconversion (SPDC). By pumping the SPDC source with a superposition of time bins, we prepare hyperentangled photonic ququarts of the form:

$$|\psi_{BC}\rangle = \frac{1}{2}\left(|H\ t_1 H\ t_1\rangle + |V\ t_1 V\ t_1\rangle + |H\ t_2 H\ t_2\rangle + |V\ t_2 V\ t_2\rangle\right), \quad (3)$$

the 4-dimensional case of (2). To execute SDT, Charles uses liquid crystals to apply phases φ_1, φ_2, and φ_3 respectively on the 2nd, 3rd, and 4th terms in the state (3). Charles' photon then travels through Alice's measurement setup and is collected into single-mode fiber-coupled silicon avalanche photodiodes for detection (detection efficiency ~45%). At present, the outcome of Alice's measurement is not broadcast to Bob for him to execute the required unitary operation; instead, Bob makes various projective measurements on the photons he receives to tomographically reconstruct what state is received, and that state, after numerically applying the appropriate unitary transformation (multiplying one of the terms by -1) based on Alice's measurement result, is compared with Charles' initial state. Those projection measurements are carried out by rotatable half and quarter waveplates, an unbalanced interferometer (whose path imbalance matches $|t_2\rangle - |t_1\rangle$), and a removable polarizer (only needed for a subset of the projections). The photons that are transmitted through the measurement system are coupled into single-mode fibers and detected by WSi superconducting nanowire single photon detectors (SNSPD) optimized for 1550nm. The SNSPD system detection efficiency is ~80%. To maintain a constant phase between $|t_1\rangle$ and $|t_2\rangle$, the secondary output port of the pump time-bin interferometer is directed into each analyzer interferometer. The output signals from the silicon photodiodes are used in a proportional-integral feedback algorithm to move a piezo-actuated translation stage that stabilizes the phase. There is an independent stabilization system for each analyzer interferometer.

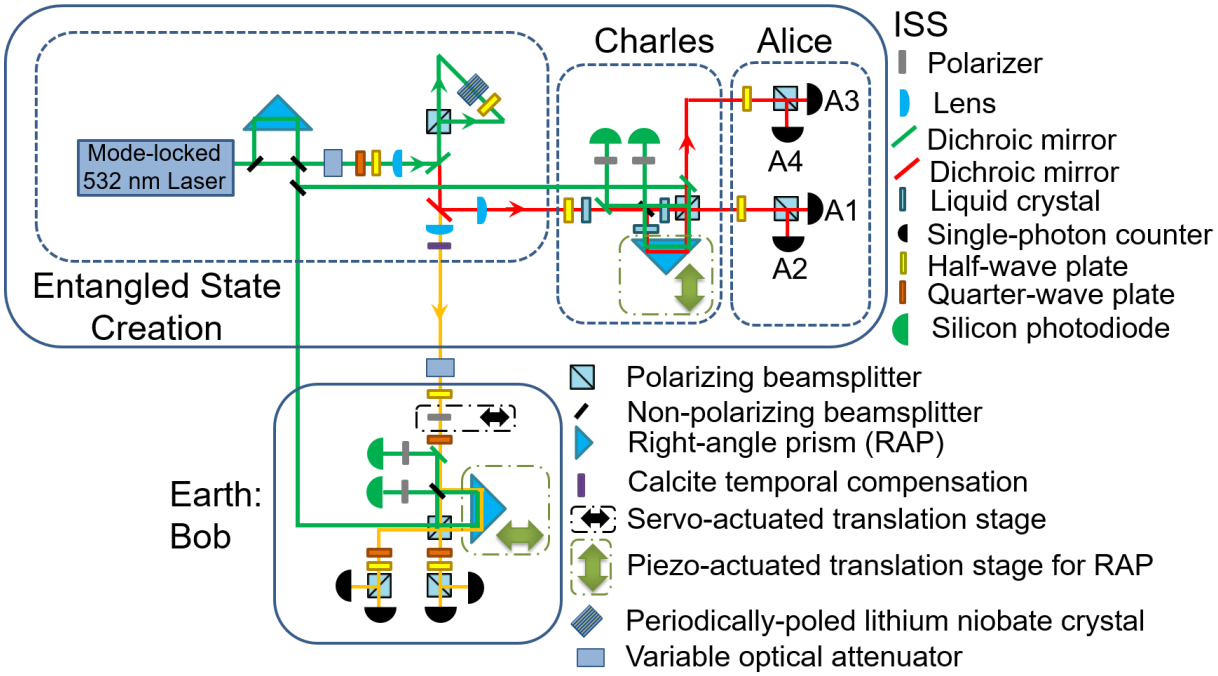

Figure 1. Optical setup to create, prepare, and measure the equimodular, hyperentangled photonic states used for SDT.

2.3 Informationally Complete Tomography System

Our previous tomography system could not measure an informationally complete set of measurements to be used in a maximum likelihood reconstruction. With the logical assumption that the photons were born in the same laser pulse, we determined it would have minimal effect on the tomography output[5]. Nevertheless, to eliminate any possible source of additional error, we have incorporated the ability to make an additional type of projective measurement, thereby making

our tomography informationally complete: Previously, we could not make projections of the type $\frac{1}{\sqrt{2}}\left(|H\ t_1\rangle + |H\ t_2\rangle e^{i\varphi}\right)$ but adding a removable polarizer and modifying the waveplate angles now allows this projection.

2.4 Reconstructed States

Alice measures the photon given to her by Charles, projecting it onto one of four basis states, depending on which of her detectors fire:

$$|A1\rangle = \frac{1}{2}\left(|H\ t_1\rangle + |V\ t_1\rangle + |H\ t_2\rangle - |V\ t_2\rangle\right) \tag{4}$$

$$|A2\rangle = \frac{1}{2}\left(|H\ t_1\rangle + |V\ t_1\rangle - |H\ t_2\rangle + |V\ t_2\rangle\right) \tag{5}$$

$$|A3\rangle = \frac{1}{2}\left(|H\ t_1\rangle - |V\ t_1\rangle + |H\ t_2\rangle + |V\ t_2\rangle\right) \tag{6}$$

$$|A4\rangle = \frac{1}{2}\left(-|H\ t_1\rangle + |V\ t_1\rangle + |H\ t_2\rangle + |V\ t_2\rangle\right). \tag{7}$$

In terms of these basis states, the total state for the photon pair shared between Alice and Bob is:

$$\begin{aligned}\frac{1}{4}[&|A1\rangle\left(|H\ t_1\rangle + |V\ t_1\rangle e^{i\varphi_1} + |H\ t_2\rangle e^{i\varphi_2} - |V\ t_2\rangle e^{i\varphi_3}\right) + \\ &|A2\rangle\left(|H\ t_1\rangle + |V\ t_1\rangle e^{i\varphi_1} - |H\ t_2\rangle e^{i\varphi_2} + |V\ t_2\rangle e^{i\varphi_3}\right) + \\ &|A3\rangle\left(|H\ t_1\rangle - |V\ t_1\rangle e^{i\varphi_1} + |H\ t_2\rangle e^{i\varphi_2} + |V\ t_2\rangle e^{i\varphi_3}\right) + \\ &|A4\rangle\left(-|H\ t_1\rangle + |V\ t_1\rangle e^{i\varphi_1} + |H\ t_2\rangle e^{i\varphi_2} + |V\ t_2\rangle e^{i\varphi_3}\right)].\end{aligned} \tag{8}$$

Thus, we see that conditional on Alice's measurement outcome, Bob will possess the desired state from Charles, modulo a minus sign on one of the four terms[5].

In Table 1, the expected and average received phases are compared for each of the four possible states sent to Bob (corresponding to Alice's four measurement outcomes) for a certain choice of $\varphi_1, \varphi_2,$ and φ_3, along with the fidelity between the states. Because some of the non-ideal components contribute extra phase shifts, a phase calibration step is required; those phase shifts are taken into account in the calculation of the expected phases. States characterized by $\varphi_1, \varphi_2,$ and φ_3 can be represented in a state space with the topology of a hypertorus. Figure 3 shows a graphical representation of the states received by Bob, labelled by Alice's measurement outcomes, in a projection of this hypertoroidal space where one dimension is represented as color. Furthermore, for additional comparison the real parts of the density matrices of the expected and received states are shown in Figure 3.

Table 1. Analysis of 4 states projected onto during SDT protocol execution; estimated standard deviations of phase uncertainties are 4°. *ACS = accidental coincidence subtraction.

Alice's State	Expected Phases			Average Received Phases			Average Fidelity	
	φ_1	φ_2	φ_3	φ_1	φ_2	φ_3	w/o ACS*	w/ ACS*
A1	74°	229°	300°	79°	218°	296°	0.939(6)	0.948(7)
A2	60°	228°	286°	65°	222°	286°	0.931(5)	0.941(5)
A3	76°	296°	360°	78°	283°	354°	0.94(1)	0.95(1)
A4	57°	282°	345°	62°	276°	343°	0.915(7)	0.925(7)

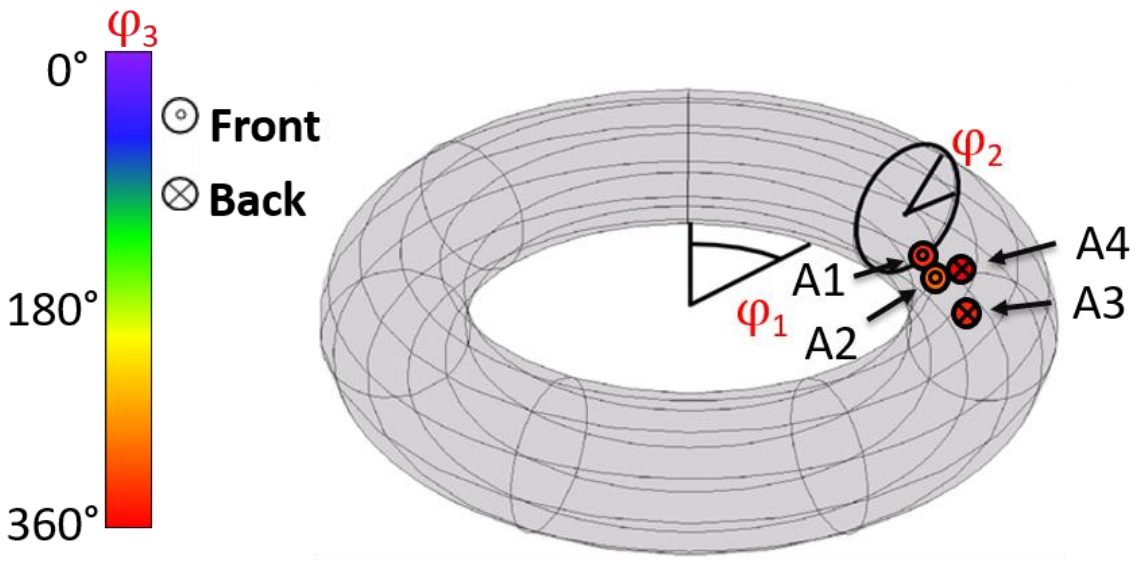

Figure 2. Graphical representation of the states received by Bob, labelled by Alice's measurement outcome, in the hypertorus phase space with one dimension as color.

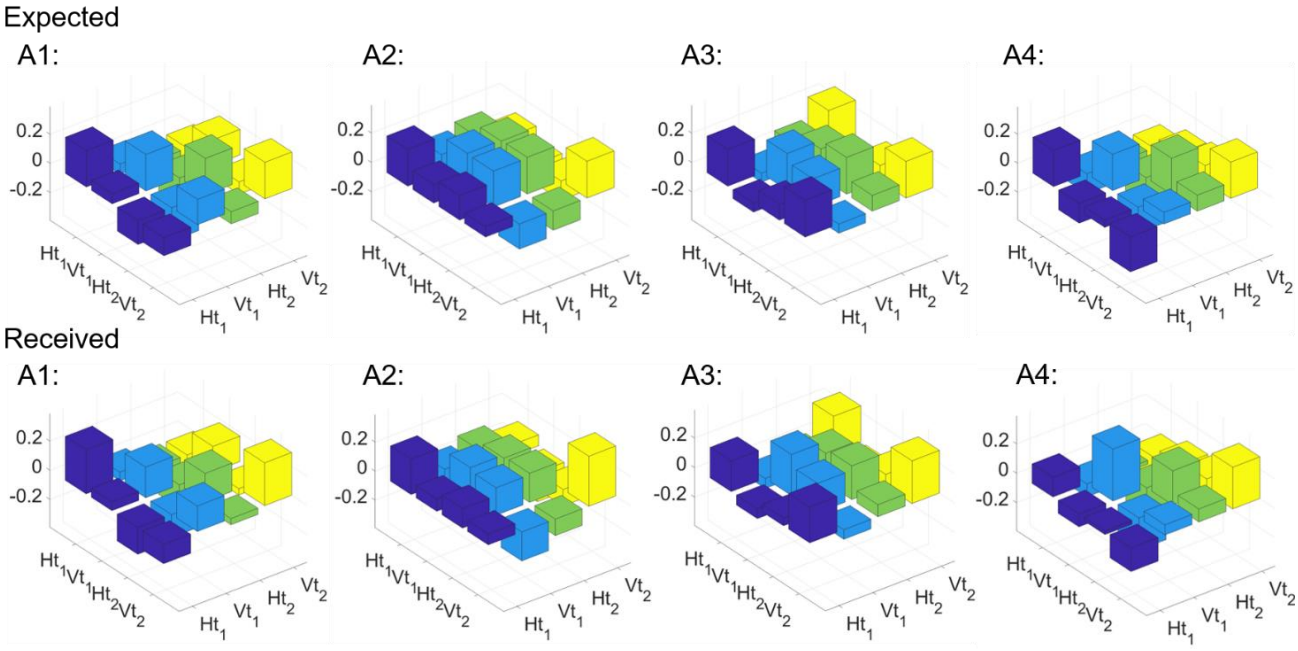

Figure 3. Real part of expected and reconstructed density matrices for the states received by Bob, labelled by Alice's measurement outcome.

3. LOOKING FORWARD TO SPACE DEPLOYMENT

Going from a table-top experiment to deployment in space involves many challenges, some of which include: the channel between Alice/Charles and Bob will have low transmission; given a finite link time, the optimum pump power must be determined; and a robust entanglement source must be developed.

3.1 Effect of Multiple Pair Events on Tomographic Reconstruction

As the pump power of an SPDC source is increased, the emission probability of an entangled pair rises, but so does the probability of emitting multiple pairs simultaneously[6]. Even with photon-number-resolving detectors and perfect transmission our experiment is adversely effected by these multiple pair events. A system with low transmission is also affected because there is a high probability that photons will be lost, resulting in uncorrelated photons being detected as coincidences. In the appendix is our analysis of the detection rates of a photon pair source by "bucket" detectors (distinguishing 0 and ≥ 1 photons). To investigate the adverse effects of multiple pair events when using "bucket" detectors like ours, Figure 4 shows the fidelity and the phase error, δφ, for the same set of phases measured for multiple values of P_p. P_p was calculated by solving (18-20), assuming no false counts (background photon(s) or intrinsic dark counts) on the detectors. Although the fidelity increases for lower P_p because the accidental coincidences are minimized, the coincidence counts collected are proportional to P_p. The lower values of P_p allow for a higher fidelity if enough coincidences can be collected during an orbital pass to not adversely affect the fidelity.

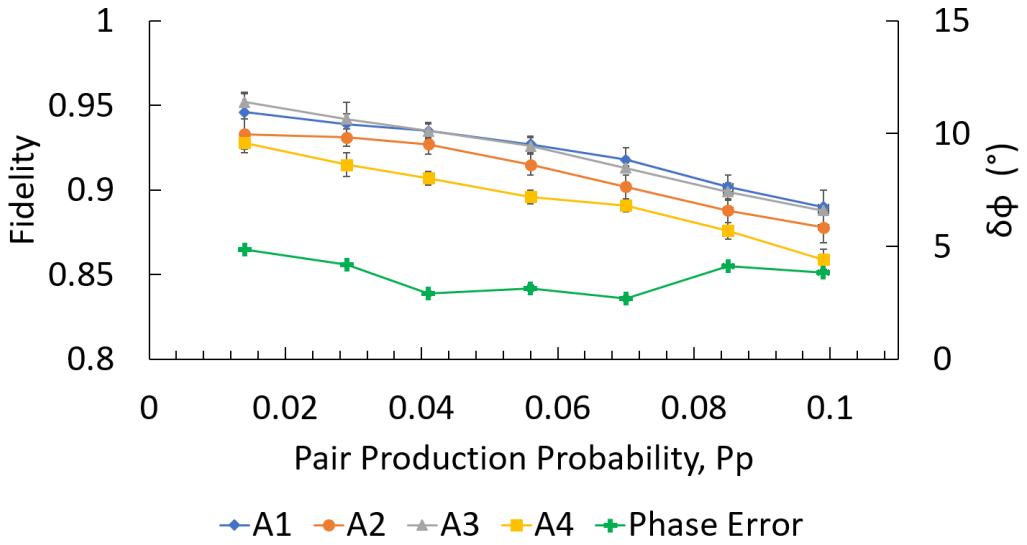

Figure 4. Fidelity and phase error of Bob's reconstructed state with Charles intended state, conditional on Alice's possible measurement outcomes A1-A4 (left y-axis), and the average estimated phase uncertainty δφ (right y-axis) plotted versus pair production probability per laser pulse.

3.2 Tomographic Reconstruction Performance

Given a finite link time during an orbital pass, low channel transmission will bound how many coincidences can be used in the tomographic reconstruction of a state sent from space to earth. Figure 5 shows the performance of our maximum likelihood tomography system versus total coincidence counts detected per tomography. Each η in equations (18-20) can be split into several contributing factors including, but not limited to: detection efficiency, fiber coupling efficiency, transmission through various optics, and free-space channel transmission. Therefore, the exact number of coincidences detected is highly system dependent. Figure 5 is plotted vs total coincidences to make the result easier to translate to other systems with different operating parameters. In our lab experiment, $R = 80$ MHz, $P_p = 0.041$, and $\eta_A \cong -17$ dB; we then varied η_B from -20 dB to -55 dB. It is interesting to note that the fidelity decreases less than 10% before the phase error quadruples, showing that phase error is a more sensitive metric of performance than fidelity in this low coincidence regime.

3.3 Waveguide-based SPDC Source Characterization

Any precise optical setup expected to perform well in space must have a robust alignment to survive the launch and the orbital environment, which can include large temperature fluctuations and vibrational shocks. To that end, we are pursuing a waveguide-based entanglement source to replace the free-space Sagnac-type source we use now. Our collaborators at AdvR, Inc. have supplied us with a dual-section periodicallypoled potassium titanyl phosphate (PPKTP) waveguide with

type-II phase matching for non-degenerate spontaneous parametric downconversion pumped by 532-nm light. When properly optimized, it should produce polarization entangled photon pairs at 810 nm and 1550 nm[7], with $|H\rangle_{810}|V\rangle_{1550}$ pairs produced in the first half of the waveguide and $|V\rangle_{810}|H\rangle_{1550}$ in the second half of the waveguide.

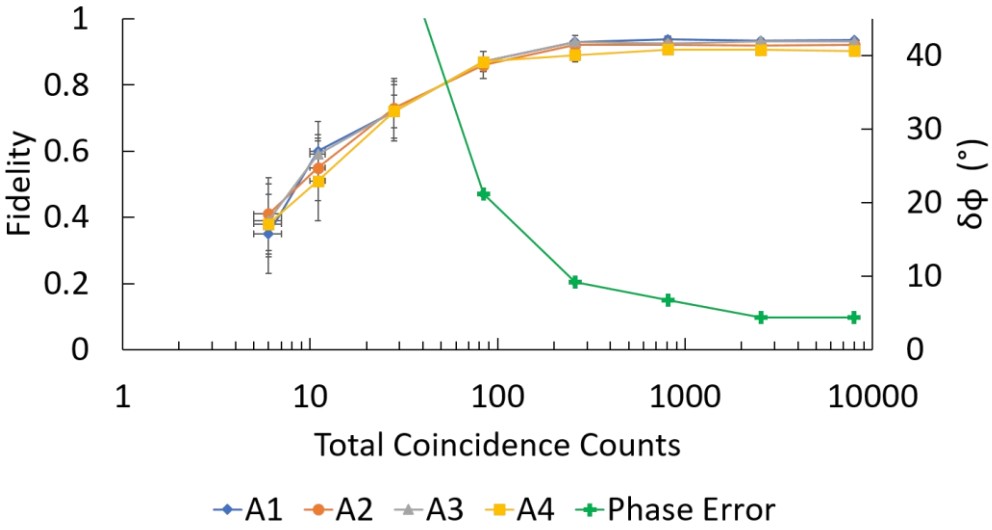

Figure 5. Fidelity and phase error of Bob's reconstructed states, plotted versus total coincidence counts detected per tomography.

We have measured coincidences from both processes of the type-II downconversion and found them to be quite unbalanced. After measuring the spectral characteristics of the two processes, we discovered that they have different bandwidths: ~8 nm for the $|H\rangle_{810}|V\rangle_{1550}$ process, ~3 nm for the $|V\rangle_{810}|H\rangle_{1550}$ process. Additionally, the entanglement visibility in the D/A basis was measured and was found to be quite low, <20%. Calculations of the polarization-dependent temporal displacement from the birefringence of the waveguide indicate that the low D/A visibility may be remedied with temporal compensation crystals unless there is some other, additional cause. Work is ongoing to characterize the different aspects of the waveguide-based SPDC source and improve its performance.

4. CONCLUSION

For long-distance quantum communication to be possible without quantum repeaters, it is necessary create a link between earth and orbiting platform to take advantage of the reduced channel loss. We have developed a system to test the execution of SDT in conditions that simulate this channel. We have shown high fidelity operation of SDT with all detectors involved in the setup. We found the relationship between pair emission probability and the fidelity of the reconstructed state and the relationship between the tomographic reconstruction accuracy and received coincidence counts, which can bound the allowable channel loss in a link budget given a desired fidelity. Additionally, we have begun the characterization of a waveguide-based entangled photon source. Initial results show the need for improvement; that work is ongoing.

5. APPENDIX: DETECTION OF MULTIPLE PAIRS

As previously mentioned, when the pump power of an SPDC source is increased, the emission probability of an entangled pair rises, but so does the probability of emitting multiple pairs simultaneously[6]. This motivates an analysis of the photon detection recorded by photon-number-resolving detectors and normal "bucket" or "click" detectors.

We start by examining the binomial expansion,

$$(x+y)^m = \sum_{k=0}^{m}\left[\binom{m}{k}x^k y^{m-k}\right], \tag{9}$$

for $x = \eta$ and $y = (1-\eta)$, where η is the detection probability:

$$\left(\eta + (1-\eta)\right)^m = \sum_{k=0}^{m}\left[\binom{m}{k}\eta^k(1-\eta)^{m-k}\right]. \tag{10}$$

(10) includes all combinations of photons from the pairs being detected or lost, because each term in the binomial expansion corresponds to a certain number of photons being detected. Additionally, this can also be seen because η is a probability and $\left(\eta + (1-\eta)\right)^m = 1$.

By separating out the terms of the sum in (10), we can model detection events by photon-number-resolving detectors. For a detection event where Alice detects α photons and Bob detects β photons, we have the following rates for Alice, Bob, and Alice and Bob simultaneously,

$$R_A(\alpha, \eta_A, P_{\alpha FC}) = R\sum_{m=1}^{\infty}\left[{P_p}^m \binom{m}{\alpha}{\eta_A}^{\alpha}(1-\eta_A)^{m-\alpha}\right] + R\,P_{\alpha FC}, \tag{11}$$

$$R_B(\beta, \eta_B, P_{\beta FC}) = R\sum_{m=1}^{\infty}\left[{P_p}^m \binom{m}{\beta}{\eta_B}^{\beta}(1-\eta_B)^{m-\beta}\right] + R\,P_{\beta FC}, \tag{12}$$

$$\begin{aligned} R_{AB}(\alpha, \beta, \eta_A, \eta_B, P_{\alpha FC}, P_{\beta FC}) = {} & R\sum_{m=1}^{\infty}\left[{P_p}^m \binom{m}{\alpha}{\eta_A}^{\alpha}(1-\eta_A)^{m-\alpha}\binom{m}{\beta}{\eta_B}^{\beta}(1-\eta_B)^{m-\beta}\right] \\ & + R_A(\alpha, \eta_A, P_{\alpha FC})\,P_{\beta FC} + R_B(\beta, \eta_B, P_{\beta FC})\,P_{\alpha FC} - RP_{\alpha FC}P_{\beta FC}. \end{aligned} \tag{13}$$

Here R is the repetition rate of the laser, P_p is the pair production probability per laser pulse, η_A (η_B) is the total transmission on Alice's (Bob's) side from pair creation to detection, and $P_{\alpha FC}$ ($P_{\beta FC}$) is the probability per laser pulse that Alice's (Bob's) detector detects an α (β) false count event (either background photon(s) or intrinsic dark count). These relations apply assuming the detector can resolve any number of photons. For realistic detectors, there is usually some upper threshold, γ_{max}, above which the detector can no longer distinguish, e.g., γ_{max} and $\gamma_{max}+1$ photons. If we assume such a detector acts like a "bucket" detector (i.e., detections of photons where $\gamma \geq \gamma_{max}$ all register the same as γ_{max}), for $\gamma \geq \gamma_{max}$ we have

$$R_A(\gamma_{max}, \eta_A, P_{A\gamma FC}) = R\sum_{m=1}^{\infty}\left[{P_p}^m \sum_{k=\gamma_{max}}^{m}\left[\binom{m}{k}{\eta_A}^k(1-\eta_A)^{m-k}\right]\right] + R\,P_{A\gamma FC}, \tag{14}$$

$$R_B(\gamma_{max}, \eta_B, P_{B\gamma FC}) = R\sum_{m=1}^{\infty}\left[{P_p}^m \sum_{k=\gamma_{max}}^{m}\left[\binom{m}{k}{\eta_B}^k(1-\eta_B)^{m-k}\right]\right] + R\,P_{B\gamma FC}, \tag{15}$$

$$\begin{aligned} R_{AB}(\gamma_{max}, \eta_A, \eta_B, P_{A\gamma FC}, P_{B\gamma FC}) = {} & R\sum_{m=1}^{\infty}\left[{P_p}^m \sum_{k=\gamma_{max}}^{m}\left[\binom{m}{k}{\eta_A}^k(1-\eta_A)^{m-k}\right]\sum_{k=\gamma_{max}}^{m}\left[\binom{m}{k}{\eta_B}^k(1-\eta_B)^{m-k}\right]\right] \\ & + R_A(\gamma_{max}, \eta_A, P_{A\gamma FC})\,P_{B\gamma FC} + R_B(\gamma_{max}, \eta_B, P_{B\gamma FC})P_{A\gamma FC} - RP_{A\gamma FC}\,P_{B\gamma FC}. \end{aligned} \tag{16}$$

We can also use these general relations to consider the case of a normal "bucket" detector, which is a special case of the formulas above for $\gamma_{max} = 1$. In that case we have

$$\sum_{k=1}^{m}\left[\binom{m}{k}\eta^k(1-\eta)^{m-k}\right] = 1-(1-\eta)^m \tag{17}$$

which is the probability of at least one photon being detected (i.e., one minus the probability that all m photons are undetected). Photons emitted from a pair source and detected by such a detector then obey these relations:

$$S_A = R\sum_{m=1}^{\infty}\left[{P_p}^m\left(1-(1-\eta_A)^m\right)\right] + R\,P_{AFC}, \tag{18}$$

$$S_B = R\sum_{m=1}^{\infty}\left[{P_p}^m\left(1-(1-\eta_B)^m\right)\right] + R\,P_{BFC}, \tag{19}$$

$$C_{AB} = R\sum_{m=1}^{\infty}\left[{P_p}^m\left(1-(1-\eta_A)^m\right)\left(1-(1-\eta_B)^m\right)\right] + S_A\,P_{BFC} + S_B\,P_{AFC} - R\,P_{AFC}P_{BFC}. \tag{20}$$

Here, S_A is the rate of one or more photons detected by Alice (Alices's singles), S_B is the rate of one or more photons detected by Bob (Bob's singles), C_{AB} is the rate of coincidentally detecting at least one photon by Alice and Bob (coincidences), and P_{AFC} (P_{BFC}) is the probability per laser pulse that Alice's (Bob's) detector detects a false count event (either background photon(s) or intrinsic dark count). Since C_{AB} includes events of uncorrelated photons, it is a measure of the total amount of coincidences detected. Only a subset of these are useful for quantum information applications, but because there is in general no way to extract or identify that subset, the effect is to reduce the measurable quantum correlation (in the simplest example, photons from two different pairs of entangled photons have no correlations between them).

6. ACKNOWLEDGEMENTS

This work was primarily supported by NASA Grant No. NNX16AM26G and this work was supported under and awarded by DoD, Air Force Office of Scientific Research, Office of Naval Research, National Defense Science and Engineering Graduate Fellowship (NDSEG).

7. REFERENCES

[1] Villoresi, P., et al. "Experimental verification of the feasibility of a quantum channel between space and Earth." New J. of Phys., **10.3**, 033038 (2008).
[2] Yin, J. et al., "Satellite-based entanglement distribution over 1200 kilometers", Science, **35**, 6343 (2017).
[3] Bernstein, H., "Superdense quantum teleportation", Quant. Info. Processing, **5**, 451-461 (2006).
[4] Graham, T. M., et al., "Superdense teleportation using hyperentangled photons," Nat. Comm., **6**, 7185 (2015).
[5] Graham, T. M., "Using Hyperentanglement for advanced quantum communication", PhD. Dissertation, University of Illinois at Urbana-Champaign, (2016).
[6] Caprara, V. V., et al., "Challenging preconceptions about Bell tests with photon pairs," Phys. Rev. A, **91**, 012107, (2015).
[7] AdvR, Inc. Bozeman, MT, USA.